IEEE Access
Multidisciplinary | Rapid Review | Open Access Journal

Received January 25, 2021, accepted January 31, 2021, date of publication February 3, 2021, date of current version February 10, 2021.

Digital Object Identifier 10.1109/ACCESS.2021.3056905

Gain Optimization of Low-Profile Textile Antennas Using CMA and Active Mode Subtraction Method

BASHAR BAHAA QAS ELIAS[1], (Member, IEEE), PING JACK SOH[1], (Senior Member, IEEE), AZREMI ABDULLAH AL-HADI[1], (Senior Member, IEEE), AND PRAYOOT AKKARAEKTHALIN[2], (Member, IEEE)

[1]Advanced Communication Engineering (ACE) CoE, Faculty of Electronic Engineering Technology, Universiti Malaysia Perlis (UniMAP), Arau 02600, Malaysia
[2]Department of Electrical and Computer Engineering, Faculty of Engineering, King Mongkut's University of Technology North Bangkok (KMUTNB), Bangkok 10800, Thailand

Corresponding authors: Ping Jack Soh (pjsoh@unimap.edu.my) and Prayoot Akkaraekthalin (prayoot.a@eng.kmutnb.ac.th)

This work was supported in part by the Ministry of Higher Education (MOHE) Malaysia through the Fundamental Research Grant Scheme under Grant FRGS/1/2020/TK0/UNIMAP/02/19, and in part by the King Mongkut's University of Technology North Bangkok under Grant KMUTNB-64-KNOW-46.

ABSTRACT This paper presents an active mode subtraction method based on the characteristic mode analysis to estimate the forward directivity based on the difference in modal significance curves. This made the optimization of the antenna gain in the design process to be more efficient. To the best of the authors' knowledge, such method is innovative and proposed in literature for the first time. This method is derived on the basis that the total radiated field of the antenna, and consequently, the directivity is mainly contributed by the excited dominant modes. To demonstrate its effectiveness, three compact, planar, and wearable antennas with increasing complexity will be designed and optimized using this method. The first is a conventional circular patch antenna operating at 5.3 GHz, whereas the second one is a planar loop antenna operating at 3.08 GHz. The third design is a crown-shaped planar antenna (CPA) with a 3 × 3 artificial magnetic conductor (AMC) plane integrated underneath to reduce potential coupling effects from the body. All three antennas are made fully using textiles with the same thicknesses: felt fabric as its substrate and ShieldIt Super as its conductive textile. For all designs, the use of the proposed method, which is validated using the method of moments, has predicted the maximum direction of radiation and its respective gain at the desired frequencies with good accuracy. Besides that, the design of the AMC plane for the CPA is also optimized using CMA prior to the integration with the antenna and a leather wrist strap. Measurements of the final crown-shaped antenna design indicated a good agreement with simulations, with an operating bandwidth of more than 240 MHz, FBR of 15.73 dB and a directional radiation pattern outward from the body.

INDEX TERMS Characteristic mode analysis, wearable antennas, textile antennas, artificial magnetic conductors.

I. INTRODUCTION

Microstrip antennas are widely used due to their low profile, lightweight, low fabrication cost and ease of integration with printed circuit board designs [1], [2]. In recent years, flexible electronic devices have especially become important to cater to the various wireless communication applications such as the internet of things (IoT), emergency services, medical and military [3], [4]. Wearable antennas are typically implemented to support the wireless communication capability in such electronic devices. They are designed using flexible materials to ease their integration with clothing when placed on various body locations such as on the chest, wrist, head, etc. This enables the sensing and monitoring the parameters from a person such as heart rate [5]. Furthermore, flexible materials such as textiles are low in relative permittivity, which potentially increases antenna bandwidth and reduces the surface wave losses [6].

The associate editor coordinating the review of this manuscript and approving it for publication was Kai-Da Xu.

Various techniques have been proposed to make the antenna design process more efficient. Moreover, as the need for smaller and multi-functional wireless devices increases, the incorporation of various techniques onto the design of an antenna radiator to achieve such objectives complicates the optimization process of the antenna. Examples of techniques to enable miniaturization and bandwidth widening include the incorporation of slots onto the antenna patch and metamaterial-based methods [7]. One of the popular types of metamaterials in planar form is the artificial magnetic conductor (AMC). They are typically used as the ground plane of an antenna to increase gain of the major lobe and decrease the undesirable back radiation [8]. This is due to the unique properties of AMC, which enable the reflection of incident electric field without changing the phase of the incident wave. This property can be used to improve the directivity of the antenna, thereby improving gain [9].

Characteristic mode analysis (CMA) is a suitable method for designing the antenna structure. The theory of CMA was first introduced in [10] and later refined in [11], [12]. Its parameters which include the modal significance, eigenvalue, and the characteristic angle, enable the visualization of modes and individual current flows. This is due to the capability of CMA in providing a set of orthogonal currents characteristic, which modes are numerically obtained for conductive bodies. These modes are only related to structure of the antenna, its size, and its operating frequency. This enables CMA to provide a physical explanation of the antenna radiation, thus facilitating the understanding of the structure for an efficient antenna design, synthesis and optimization [13].

In this paper, a method to optimize gain and directivity by studying the active modes from different radiating structures using CMA is proposed. This method, referred to as the active mode subtraction (AMS) method, is based on the principle of subtracting the magnitudes of the electric fields of the dominant modes. To determine the dominant modes, the modal significance of the structure is first observed at the desired frequency using CMA. To efficiently optimize the gain/directivity, AMS values are evaluated at different directions (relative to the forward direction). These evaluations are also performed for different dominant modes at a common resonant frequency. This is performed on the basis that the total radiated field of the antenna, and consequently, the directivity is mainly determined by the dominant modes [14]. Thus, the radiation patterns generated are resulting from the combination of the excited dominant modes [15], [16]. To the best of the authors' knowledge, such method for this purpose is innovative and proposed in literature for the first time.

The proposed technique is demonstrated on three practical and unique wearable antenna topologies, as follows:

- Design 1: a conventional circular patch antenna.
- Design 2: a planar loop antenna.
- Design 3: a crown-shaped patch antenna.

Results from simulations using CMA and method of moments (MoM), and measurements for both prototypes will be presented to validate this method. Furthermore, the application of the CMA method in the antennas' design and optimization procedure will be performed systematically, including for the design and integration of a unique AMC structure in the first design. Finally, an on-body evaluation of the proposed strap-type antenna is performed via simulations and measurements, prior to the conclusion in the last section

The level of improvements due to the addition of the AMC structure is then evaluated and quantified by benchmarking against a conventional wearable patch antenna. The use of the new AMS method eases the design and behavior characterization of the proposed CPA for on-body applications and its integration with the watch strap and textile AMC structure.

II. OVERVIEW OF THE AMS METHOD USING CMA

As aforementioned, the proposed AMS method is applied as one of the important optimization steps in the antenna design steps using CMA. To apply this method, the following steps are performed:

i. The simplified more of the radiator structure is first designed without the substrate and excitations
ii. This structure is analyzed using CMA to determine the dominant modes at the target frequency. This can be determined by observing the close-to-unity modal significance.
iii. Upon determining the dominant modes of the structure, the antenna radiator is then integrated with its substrate and excitation.
iv. Surface currents are generated to understand the operation of the antenna. Optimization in the structure in terms of reflection parameters are done by observing the changes the current paths and distributions on the antenna radiator.
v. Next, the AMS method is applied to estimate the forward directivity of the antenna. This method is based on the subtraction of the magnitude of the electric fields of the two dominant modes generated from the proposed structure.
vi. The radiation patterns from the combinations of these modes are then generated by simultaneously exciting the dominant modes [15], [16]. The summations of the electric fields from each mode is then determined. These values determine the radiation behavior of the structure, which in turn, enables the prediction of the antenna directivity.
vii. When there is a small (< 1) difference between the modal significance between the two or more active modes, both of modes are properly excited, thus generating a high directivity towards the given direction.
viii. On the contrary, when this difference starts to increase (to > 1), it indicates that one of the dominant modes is not properly excited and has a lower electric field intensity along the given direction. This results in the decrease of the directive radiation of the structure due to the unequally excited dominant modes and consequently, the reduces total electric field.

In literature, most of studies applied optimization methods which are integrated within the simulation software package. They include the likes of Genetic Algorithm (GA), Adaptive Response Surface Method (ARSM), and Particle Swarm Optimization (PSO), which are also capable of optimizing antenna parameters such as the forward directivity at the specific frequencies. Several other studies have also used these optimization strategies to improve the directivity of the antenna. For example:

i. The work in [17] presented a method in optimizing the directivity in the broadside direction of a rectangular patch antenna using GA. This optimization method successfully resulted in a similar directivity as linear arrays using a corporate or series feeding.
ii. The work in [18] used the Contiguous Partition Method (CPM) to optimize the directivities of different patterns in planar monopulse array antennas. This optimization method aims to arrive at a solution closest as possible to the reference pattern with maximum directivity. A two-stage procedure is used in CPM to excite and match the structure aimed at maximum directivity as follows:
   - the optimal excitation coefficients providing different patterns with maximum directivity are first computed based on the guidelines in [18].
   - the CPM is used to match the optimal pattern, thus defining the "best solution" compromise.

As a comparison, the proposed AMS method is simpler and more flexible relative to the methods presented in literature. This is because the CMA-based method does not require the substrate layer and the excitation to be included in simulations. This enables a shorter time and optimization effort in estimating directivity of antennas, which can be implemented on different antenna structures with varying complexities.

Three design examples demonstrating the application and efficiency of this method will be explained in the forthcoming section.

III. ANTENNA DESIGNS AND CONSIDERATIONS

A. DESIGN 1: CIRCULAR PATCH ANTENNA

In the first design, a conventional circular microstrip patch structure is designed on top of a felt substrate, with a full ground plane located on its reverse side. Fig. 1 presents the geometry of the circular patch in this design. The felt substrate layer used is 3 mm in height (h), with a dielectric constant (ε_r) of 1.3 and a loss tangent (tanδ) of 0.044. ShieldIt Super®conductive textile is used to form the conducting elements in this antenna. It has a thickness of 0.17 mm and an estimated conductivity of 1.18×10^5 S/m. The radius of the patch is calculated based on the equation in [19] to obtain resonance close to 5.8 GHz, which resulted in $R1 = 13.22$ mm. The overall size of the substrate is $L1 \times W1 = 38 \times 42$ mm^2.

The width of the microstrip feed line (Wf) is optimized using the particle swarm optimization (PSO) algorithm available in FEKO [1]. The goal is focused on optimizing the antenna impedance matching while varying Wf, which is found to be best at 2.39 mm.

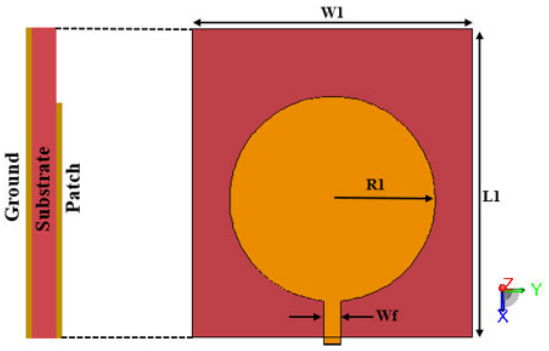

FIGURE 1. The geometry of the proposed circular patch antenna.

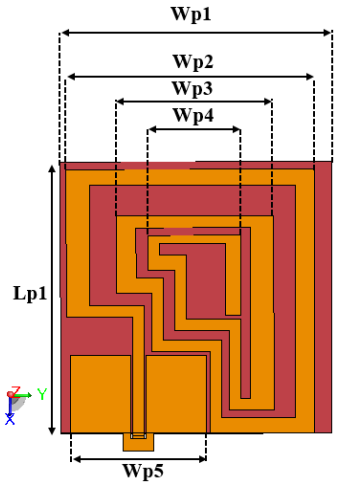

FIGURE 2. Geometry of the loop antenna.

B. DESIGN 2: PLANAR LOOP ANTENNA

The next antenna is designed based on a planar loop structure and fed using a coplanar waveguide (CPW) line, as shown in Fig. 2. The same felt substrate and ShieldIt Super conductive textile with the same thicknesses are used for this design. The radiating elements of the antenna consists of a three-turn continuous rectangular loop located on the top surface of the felt substrate (see Fig. 3). The same PSO method is used to optimize twenty significant dimensions, with an optimization reflection coefficient goal of at least -10 dB for operation at 3.08 GHz. The improved the current distributions along the surface of the radiating elements then enhanced the antenna overall performance. The CPW line feeding implemented in this design enables a single-layered design for the textile loop antenna. The gap between the feed line and the CPW enables the control of the antenna's impedance matching and must be designed with care to ensure optimized resonance. The detailed antenna dimensions are summarized in Table 1.

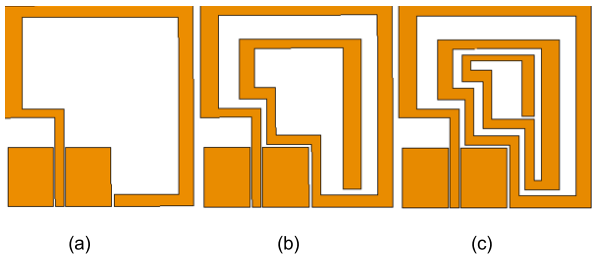

FIGURE 3. Loop antenna structure (a) one turn (b) two turns (c) three turns.

TABLE 1. Loop antenna dimensions.

Parameter	Value (mm)	Parameter	Value (mm)
LP1	70	*WP3*	40.5
WP1	70	*WP4*	24
WP2	64	*WP5*	35

TABLE 2. CPA dimensions.

Parameter	Value (mm)	Parameter	Value (mm)
W1	38	*Wf*	2.39
W2	26	*L1*	42
W3	3.18	*L2*	26
W4	7.12	*L3*	0.8
W5	2.39	*L4*	3.98
W6	8.75	*L5*	6.36
W7	10.34	*L6*	1.59
W8	19.08	*L7*	3.58
W9	6.15	*h*	3

C. DESIGN 3: CROWN-SHAPED PATCH WITH AMC PLANE

To design this antenna, Design 1 is modified to enable miniaturization and bandwidth broadening by the addition of slots. The slots are added in the following way: first, two circular slots with radii of $R2 = 1.95$ mm, and $R3 = 1.19$ mm, respectively, are inserted on the center and the top edge of the patch. Next, a small V-shaped slot positioned under the circular slot positioned on the top edge of the patch. This is followed by the insertion of a pair of lung-shaped slots on the left and right sides of the patch. Besides that, the bottom side of the patch was organized as two opposite E-shaped elements that were isolated by a large rectangular slot, as depicted in Fig. 4. These procedures, presented in four steps, will be discussed in the next section to highlight their influence on the performance of the antenna. All antenna parameters are tabulated in Table 2.

The AMC plane consists of a 3 × 3 array of diamond patch unit cells, centered on a felt substrate with dimensions. This patch is then integrated with a pair of arched burrs at the top, middle and the bottom of the patch, as shown in Fig. 5(a). The vertical distance between the middle-arched burrs of two adjacent cells is $D1 = 13$ mm, whereas the horizontal distance

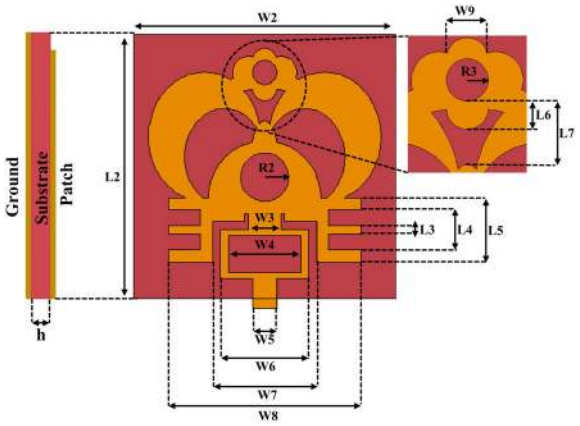

FIGURE 4. Layout of the CPA.

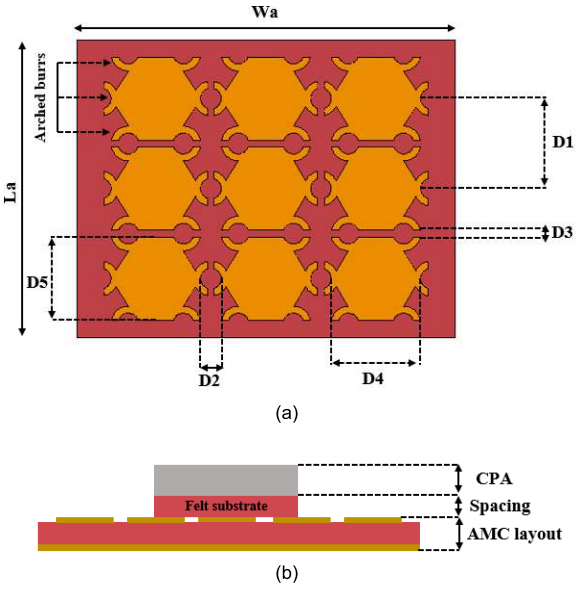

FIGURE 5. (a) 3 × 3 array AMC unit cell structure (b) Side view of the composite antenna.

between them is $D2 = 3$ mm. In addition to that, the isolation distance between the patch cells is $D3 = 1$ mm, whereas the dimensions of the diamond cell are $D4 = 13$ mm and $D5 = 12$ mm.

In general, AMC planes reflects incident E-fields without affecting its phase. Using this property, the directivity of the antenna can be increased and in turn, gain can be improved [20]. When positioned over the AMC reflector, a small spacing is preferred between this reflector and the antenna. This is to avoid the cancellation of the radiation of the currents on the antenna by the mirror image currents flowing in the opposite surface, which will consequently affect the radiation performance severely [21]. Several literatures have implemented this distance using air gaps, with its distance from the AMC or Perfect Electrical Conductor (PEC) reflector realized using vias or PCB spacers. Besides that, the same substrate material can be used as the spacer and is defined in Fig. 5(b).

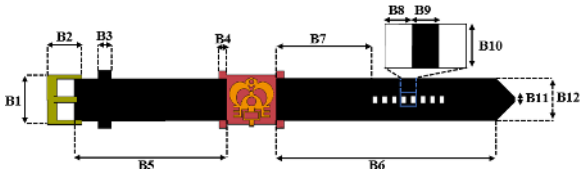

FIGURE 6. Structure of CPA with a watch strap.

TABLE 3. Strap/buckle dimensions.

Parameter	Value (mm)	Parameter	Value (mm)
B1	26	*B7*	50.5
B2	18	*B8*	2.5
B3	7	*B9*	2.5
B4	4	*B10*	4
B5	80	*B11*	2
B6	125	*B12*	22

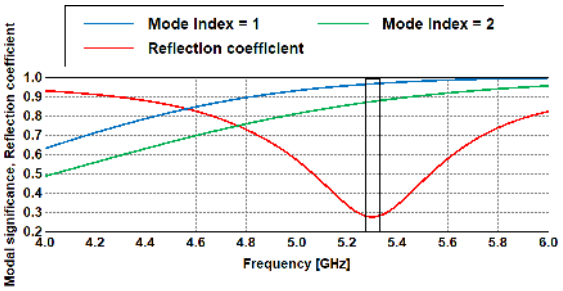

FIGURE 7. Modal significance and reflection coefficient results of circular patch antenna.

Next, the reflector plane is replaced by a strap attached to the left and right sides of the CPA to increase its practicality in wireless body area network (WBAN) applications. The strap is made of genuine leather with a dielectric constant of $\varepsilon_r = 1.8$ and thickness of 3 mm, whereas the strap/buckle is made of stainless steel with a conductivity of $\sigma = 1 \times 10^6$ S/m. The CPA with the strap is shown in Fig. 6, and the overall dimensions are illustrated in Table 3.

IV. RESULTS AND DISCUSSION

A. DESIGN 1: CIRCULAR PATCH ANTENNA

The radiation characteristics of the circular patch antenna are first analysed using CMA and MoM. Based on Fig. 7, the circular antenna exhibits a 10 dB bandwidth of 150 MHz (from 5.22 to 5.37 GHz), centered at 5.3 GHz. Besides that, the modal significance analysis of the radiator indicated that mode 1 and mode 2 are the dominant modes at the center frequency.

Next, the AMS method is applied to estimate the forward directivity of the antenna based on the CMA technique, as described in Section II. Fig. 8 show that the peak forward directivity of the antenna is obtained at $\theta = 0°$. This value gradually diminishes when towards the rest of the directions. For example, at $\theta = 0°$, the magnitude values of the electric

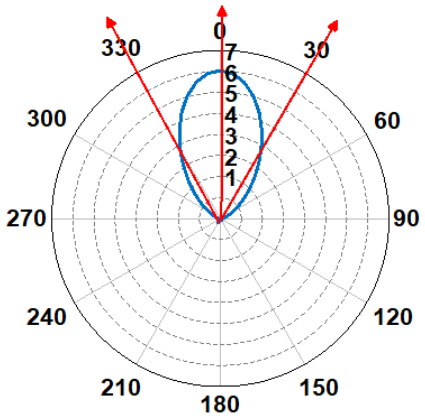

FIGURE 8. Directivity of circular patch antenna at 5.3 GHz at the x-y plane (with $\theta = 0°$).

TABLE 4. AMS status at different degrees of θ directions.

Theta (θ)	Mode 1 [V]	Mode 2 [V]	|Mode 1 – Mode 2| [V]	AMS Value	Directivity [dBi]	Realized gain [dBi]
0°	8.2	8.24	0.04	< 1	8.47	6.36
30°	6.65	7.49	0.84	< 1	5.87	3.76
60°	3.29	6.07	2.78	> 1	-1.209	-3.32
90°	0.007	5.43	5.423	> 1	-14.71	-16.82

field at the two dominant modes 1 and 2 are 8.2 V and 8.24 V, respectively. The subtraction result for these two modes is 0.04 V (less than 1), indicating a similarity between the electric field values produced by the two modes are similar. The directivity and the realized gain achieved are 8.47 dBi and 6.36 dBi, at this θ direction. Next, the separation distance between the electric field of the modes is significantly increased at $\theta = 30°$, hence, increasing the AMS result to 0.84 V. However, this value is still less than unity, with a directivity and realized gain 5.87 dBi and 3.76 dBi at this direction. When the radiation direction is changed to $\theta = 60°$ and $\theta = 90°$, the spacing between the two curves is further increased. The AMS values produced is 2.78 V and 5.42 V, respectively, which exceeds unity. The directivity and the realized gain then deteriorated to -1.209 dBi and -3.32 dBi, respectively at $\theta = 60°$, whereas at $\theta = 90°$, these values are -14.71 dBi and -16.82 dBi, respectively. Table 4 summarizes the results obtained from the AMS method at different θ directions. Based on the electric fields of the dominant modes illustrated in Fig. 9, it is observed that the electric field magnitudes of modes 1 and 2 are the closest at $\theta = 0°$. It can be also concluded that the value of AMS remains less than unity up to $\theta = 30°$ direction, which also exhibited an acceptable result of directivity and gain.

B. DESIGN 2: PLANAR LOOP ANTENNA

CMA analysis of the loop radiator indicates that mode 6 and mode 11 are the dominant modes at the initial resonant

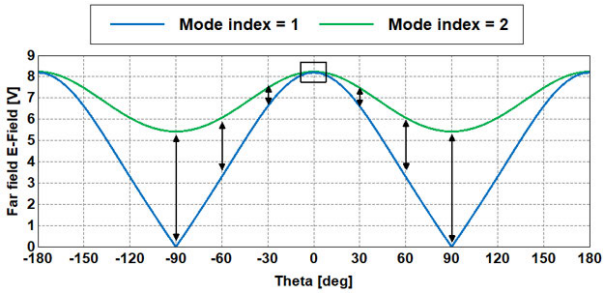

FIGURE 9. AMS calculations at different degrees of θ.

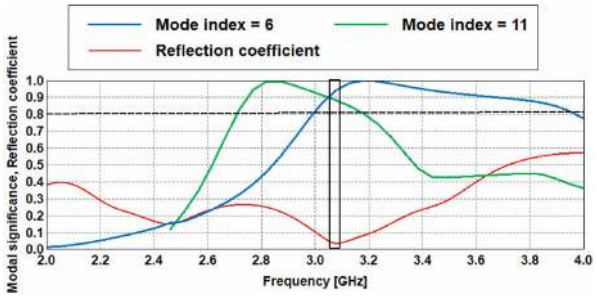

FIGURE 10. Modal significance and reflection coefficient results.

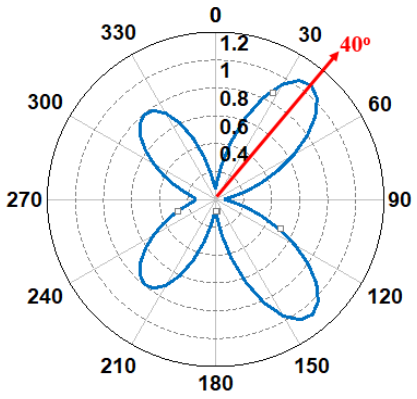

FIGURE 11. Directivity of Loop antenna at 3.08 GHz at the *x-y* plane (with $\theta = 40°$).

frequency of 3.08 GHz, as illustrated in Fig. 10. This antenna is then integrated with the substrate. Upon excitation, it is noticed that its peak directivity is directed at $\theta = 40°$, with nulls at $\theta = 0°$ and $\theta = 90°$, as depicted in Fig. 11.

Next, to optimize the directivity/gain, the magnitudes of the electric field for the two modes are subtracted at different θ directions, as shown in Fig. 12. It is seen that the minimum value of AMS is 0.03 V, produced from subtracting the two dominant modes 6 and 11 at $\theta = 40°$. At this direction, a maximum directivity of 1.02 dBi and realized gain of 0.164 dBi is produced. When the spacing between the two curves is significantly increased, the AMS value is also increased to 7.5 V (at $\theta = 0°$) and 2 V (at $\theta = 90°$). On the contrary, the directivity produced is -5.57 dBi (at $\theta = 0°$) and -5.8 dBi (at $\theta = 90°$). A realized gain of -6.42 dBi (at $\theta = 0°$) and -6.66 dBi

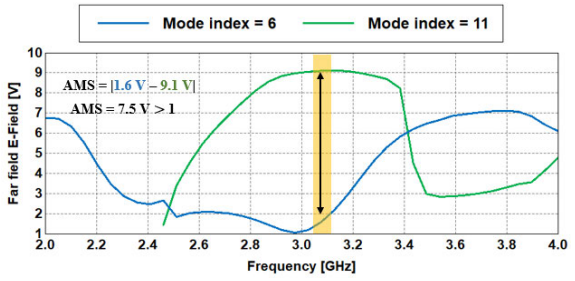

(a)

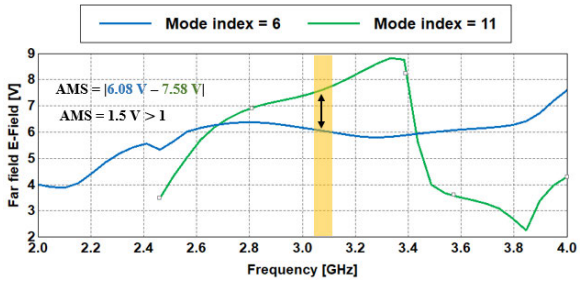

(b)

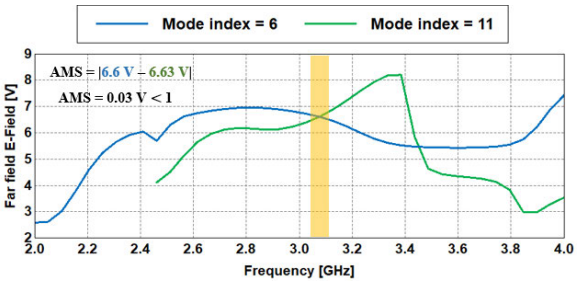

(c)

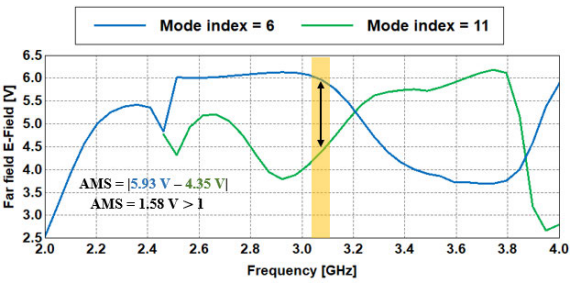

(d)

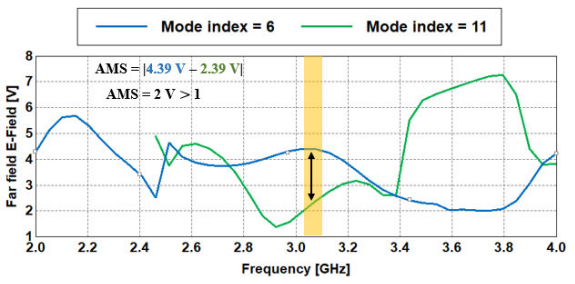

(e)

FIGURE 12. AMS calculations at different degrees of θ (a) $\theta = 0°$ (b) $\theta = 30°$ (c) $\theta = 40°$ (d) $\theta = 60°$ (e) $\theta = 90°$.

TABLE 5. AMS values at different θ directions.

Theta (θ)	Mode 6 [V]	Mode 11 [V]	|Mode 6 – Mode 11| [V]	AMS Value	Directivity [dBi]	Realised gain [dBi]
0°	1.6	9.1	7.5	> 1	-5.57	-6.42
30°	6.08	7.58	1.5	> 1	0.621	-0.276
40°	6.6	6.63	0.03	< 1	1.02	0.164
60°	5.93	4.35	1.58	> 1	-0.79	-1.57
90°	4.39	2.39	2	> 1	-5.8	-6.66

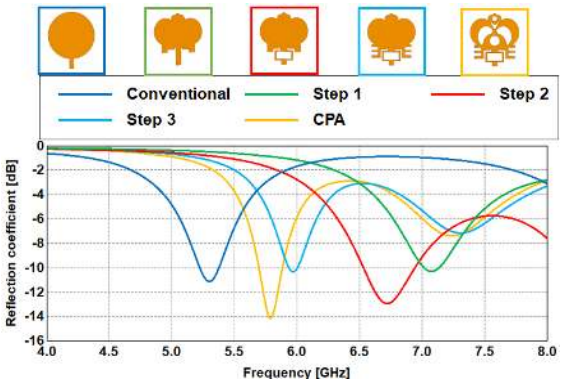

FIGURE 13. The reflection coefficients of the conventional and each design step of the proposed antenna.

(at $\theta = 90°$) is produced. Furthermore, the AMS value remained higher than 1 at $\theta = 30°$ and $\theta = 60°$, indicating 1.5 V and 1.58 V, respectively. The forward directivity and realized gain obtained is 0.621 dBi and −0.276 dBi, respectively at $\theta = 30°$, whereas its obtained −0.79 dBi and −1.57 dBi, respectively at $\theta = 60°$. Table 5 summarizes the AMS results at different degrees of θ.

C. DESIGN 3: CROWN-SHAPED PATCH WITH AMC PLANE

The proposed CPA is designed and simulated using FEKO software using MoM and CMA methods in terms of reflection coefficient, gain, surface current distribution, and radiation patterns. In Fig. 13, the reflection coefficient generated by a conventional circular antenna radiator is compared with the step by step addition of various slot structures into the proposed antenna radiator. Upon the excitation of the circular patch, it is observed that the structure is resonant at 5.3 GHz with a reflection coefficient of −11.13 dB. However, after optimization, the final CPA produced a resonance at 5.8 GHz with a reflection coefficient of −14.1 dB.

Next, the simple circular patch is modified at its patch boundaries, followed by the connection of a rectangular stub with the feed line. The rectangular slot stub technique is designed based on [22], [23], and facilitated the impedance matching between the microstrip line and the patch antenna. This consequently improving the antenna reflection coefficient. It is observed that the first step shifted the resonant frequency to 7.07 GHz, which was then gradually decreased towards the 5.8 GHz target frequency.

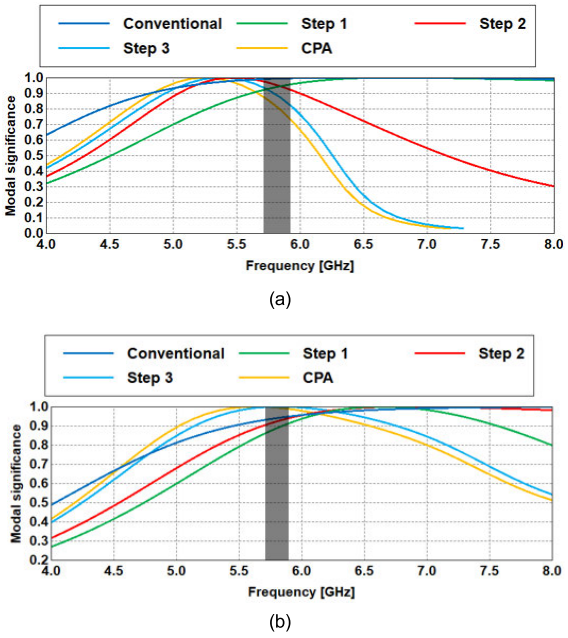

FIGURE 14. Modal significance results of the CPA (a) Mode 1 (b) Mode 2.

After that, E-shaped patches are added near the sides of the feed line. The two symmetrical E-shaped elements are designed based on [24], [25], whereas the rectangular stub element at the antenna feed is designed based on [22], [23]. Specifically, in [24] and [25], the E-shaped elements contributed to enable resonance control at the desired resonant frequency. The addition of the rectangular and the E-shaped patches have reduced the resonant frequency to 6.72 GHz and 5.97 GHz, respectively. These two techniques are then integrated with the proposed antenna structure to easily enable control of the operating frequency via parameter adjustments towards the target frequency.

Finally, a pair of circular slots and another pair of semi-circular slots are then etched onto the patch as the last step of the design procedure. The modal significance parameter from the CMA has been used to optimize other antenna elements such as the lung slots. Their locations have chosen based on the generated surface currents, and the frequency response has been evaluated at each design stage at the two dominant modes. The combination of these techniques onto the patch enabled the final design to form the final and unique crown antenna structure and achieving the required specifications. These steps considerably affected the resonant frequency and reflection coefficient of the antenna, and therefore they are considered critical steps in the optimization process in shifting the resonant frequency to 5.8 GHz.

On the other hand, design steps of the CPA using the CMA method are first performed without the substrate layer, full ground plane, and excitation. Results indicate a close-to-unity modal significance for the dominant modes of mode 1 and 2 at 5.8 GHz, as shown in Fig. 14. It is observed that the rectangular-shaped slot and the pair of E-shape radiating elements in the last three steps of the design procedure

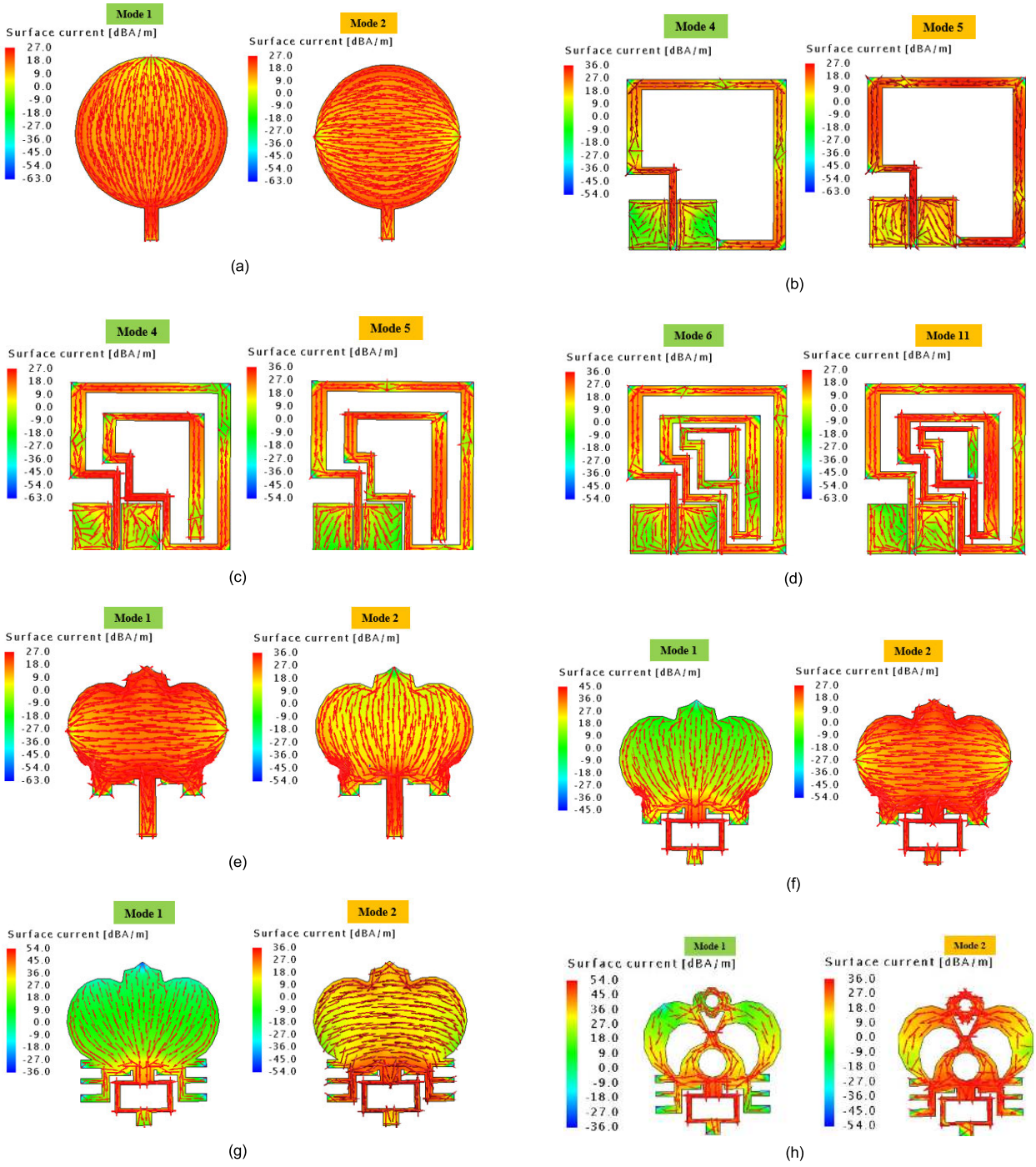

FIGURE 15. Surface current distribution of the designs (a) conventional design (b-d) loop design (e-h) CPA design.

drastically influenced the response of mode 1 of the CPA after 5.8 GHz. On the other hand, the effect of mode 2 in all steps are minimal, producing an acceptable (close to unity) value.

Fig. 15(a) presents the current distributions of the conventional circular patch design for mode 1 and mode 2 at 5.8 GHz. It is observed that the maximum current distribution along the surface of the radiator element is 27 dBA/m. In the second design with one turn, modes 4 and 5 are the dominant modes around 3.08 GHz with the surface current of 36 dBA/m and 27 dBA/m, respectively. On the contrary, in the case of two turns, it is found that the peak current distribution obtained in the first case is reversed to 27 dBA/m and 36 dBA/m for modes 4 and 5, respectively. Finally, after the adding of the third turn, the dominant modes have changed to mode 6 and 11 with the same maximum current as of the previous case of two turns. As a result, more turns

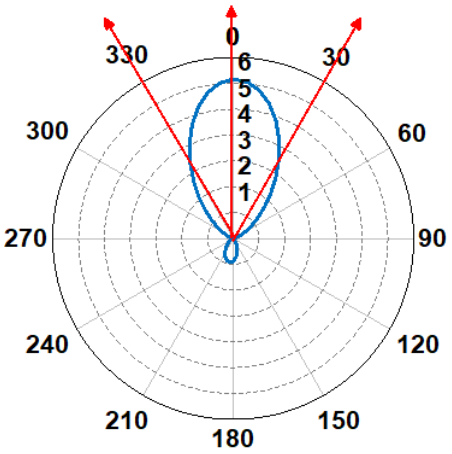

FIGURE 16. Directivity of CPA at 5.8 GHz at the *x* -*y* plane (with $\theta = 0°$).

make the surface current of the radiator more intensive as shown in Fig. 15(b-d). On the other hand, the surface current distribution of the CPA changes upon the introduction of additional elements in the design procedure. It can be summarized that the rectangular slot increases the current path of the feed line and improved the current density to 45 dBA/m for mode 1 and 27 dBA/m for mode 2, which consequently improved reflection coefficients. On the other hand, the pair of complementary E-shaped patch elements increased the surface currents in this structure to 54 dBA/m (for mode 1) and 36 dBA/m (for mode 2). Finally, the slots implemented in the last step maintained the current density distribution over the antenna surface and adjusted the operating frequency to 5.8 GHz (see Fig. 15(e-h)).

Next, the AMS method is applied to estimate the forward directivity of the antenna based on the CMA technique. As aforementioned, mode 1 and mode 2 are the dominant modes for this structure. If the value of the electric field subtraction of these modes is less than 1, that means the two modes are strongly excited and contribute significantly to the radiation pattern. On the other hand, AMS values of greater than 1 indicates that one of the dominant modes is not properly excited and has a lower electric field intensity along the given θ direction. This affects the total radiation field and considerably reduces the directivity.

It is found that the closer the subtracted AMS value to 0 V, the higher is the value of the structure's directivity, with an acceptable directivity ranging from 0 V to 1 V. As seen in Fig. 16, the highest directivity is observed at $\theta = 0°$ and decreases as the θ value changes gradually. Nonetheless, the main lobe shows a good forward directivity of approximately between $\theta = \pm 30°$. Similarly, In Fig. 17(a), the electric field subtraction of dominant modes 1 and 2 with an AMS value of 0.29 V indicated 7.89 dBi of forward directivity and 4.76 dBi of realized gain at $\theta = 0°$. This directivity is significantly decreased to 5.49 dBi and 2.35 dBi with the increase of the AMS value to 1.1 V (at $\theta = 30°$) and 2 V (at $\theta = 45°$), as shown in Fig. 17(b) and (c), respectively. The realized gain is also significantly decreased to 2.344 dBi

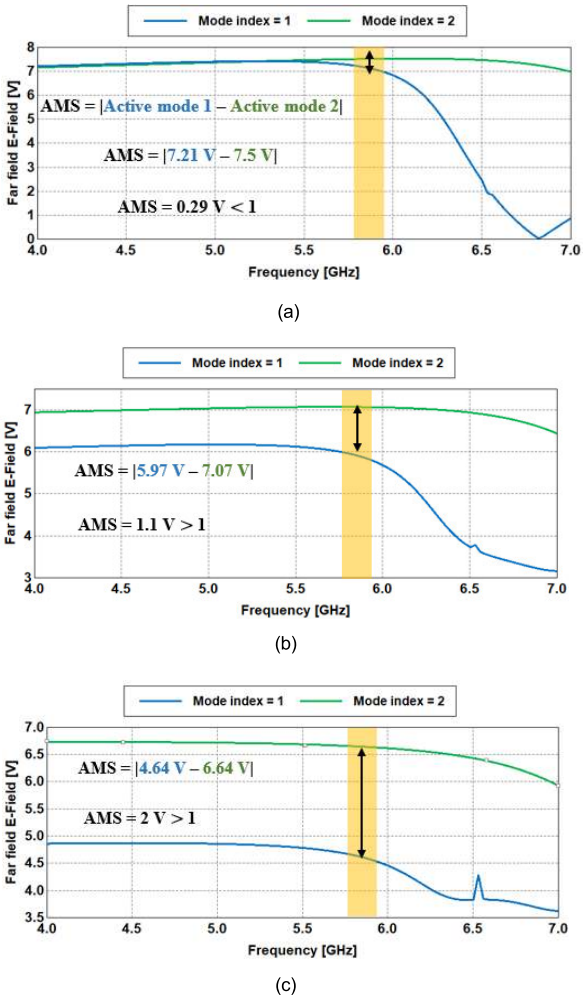

FIGURE 17. AMS calculations at different degrees of θ (a) $\theta = 0°$ (b) $\theta = 30°$ (c) $\theta = 45°$.

and -0.83 dBi at these two directions, respectively. When θ is above $\pm 30°$, the AMS value exceeds 1 V; resulting in a significant directivity degradation. It is observed that the maximum AMS value between the modes is obtained at $\theta = 90°$, producing a directivity and realised gain of -13.9 dBi and -17.07 dBi, respectively. This again indicated that the maximum directivity has been obtained when a minimum spacing between the electric field magnitudes of the two dominant modes (with AMS values of less than 1), at $\theta = 0°$. On the contrary, the AMS value increased to the 3.11 V and 5.8 V at $\theta = 60°$ and 90°, respectively, and causing the directivity to significantly decrease. Table 6 summarizes the AMS results at different θ directions.

The next stage investigates the AMC reflector characteristics using CMA. The first step involves the analyzing a conventional diamond-shaped AMC unit cell without any structural modifications. This unit cell is then integrated with arched burrs and being examined in terms of modal significance as shown in Fig. 18. The conventional AMC unit cell indicated a low efficiency in the first three modes at 5.8 GHz. After adding the arched burrs, all modes have improved, with

TABLE 6. AMS status at different degrees of θ directions.

Theta (θ)	Mode 1 [V]	Mode 2 [V]	|Mode 1 – Mode 2| [V]	AMS status	Directivity [dBi]	Realised gain [dBi]
0°	7.21	7.5	0.29	< 1	7.89	4.76
15°	6.88	7.38	0.5	< 1	7.32	4.188
25°	6.32	7.19	0.87	< 1	6.25	3.122
30°	5.97	7.07	1.1	> 1	5.49	2.344
45°	4.64	6.64	2	> 1	2.35	-0.83
60°	3.14	6.25	3.11	> 1	-2.3	-5.37
90°	0.06	5.86	5.8	> 1	-13.9	-17.07

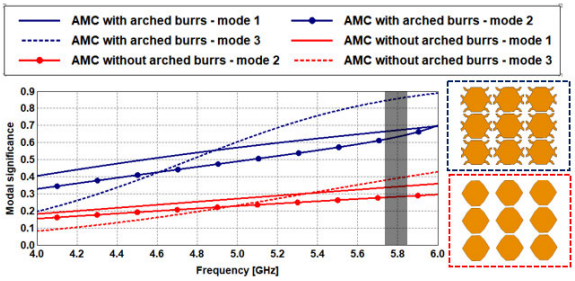

FIGURE 18. Modal significance of AMC unit cells at different modes with and without arched burrs.

mode 3 showing a peak modal significance at the resonant frequency. Next, the simulated current distribution of the proposed AMC structure is presented in Fig. 19. In mode 1, the horizontal current flow at the center of the 3 × 3 unit cell array is maximum, and gradually reduces towards other neighboring cells, except for the cells located at the corners. For mode 2, the patch unit cells positioned in the middle column showed a strong vertical current density, whereas for mode 3, the currents are distributed in all the cells more uniformly and circulate around the cell center.

Upon integration of the unit cell array and the radiator, Fig. 20 shows a low current distribution on the surface of the unit cells. This is due to the AMC plane operating as a reflector, thus reducing back radiation within the antenna's operating bandwidth. Comparison of the CPA operating with and without this 3 × 3 AMC ground indicated that both of them obtained the highest gain of 8 dBi in the three-dimensional (3D) plot with two independent θ and ϕ values, whereas the forward gain at $\theta = 0°$ is 5.17 dBi in the two-dimensional plot with a fixed ϕ value, as illustrated in Fig. 21 (a) to (c).

The CPA is then fabricated and measured with a 3 × 3 AMC array and strap watch for ease of integration into different WBAN applications, as shown in Fig. 22 (a) and (b). The experimental results have good agreement with the simulated ones in terms of reflection coefficients and radiation patterns, as illustrated in Fig. 22 (c) and (d). It can be observed that the CPA with 3 x 3 AMC reflector operates in the resonant frequency of 5.94 GHz with an impedance bandwidth of more than 200 MHz, while the simulated relative impedance bandwidth is 180 MHz. The discrepancies between the experimental and simulated results are due to factors such as the

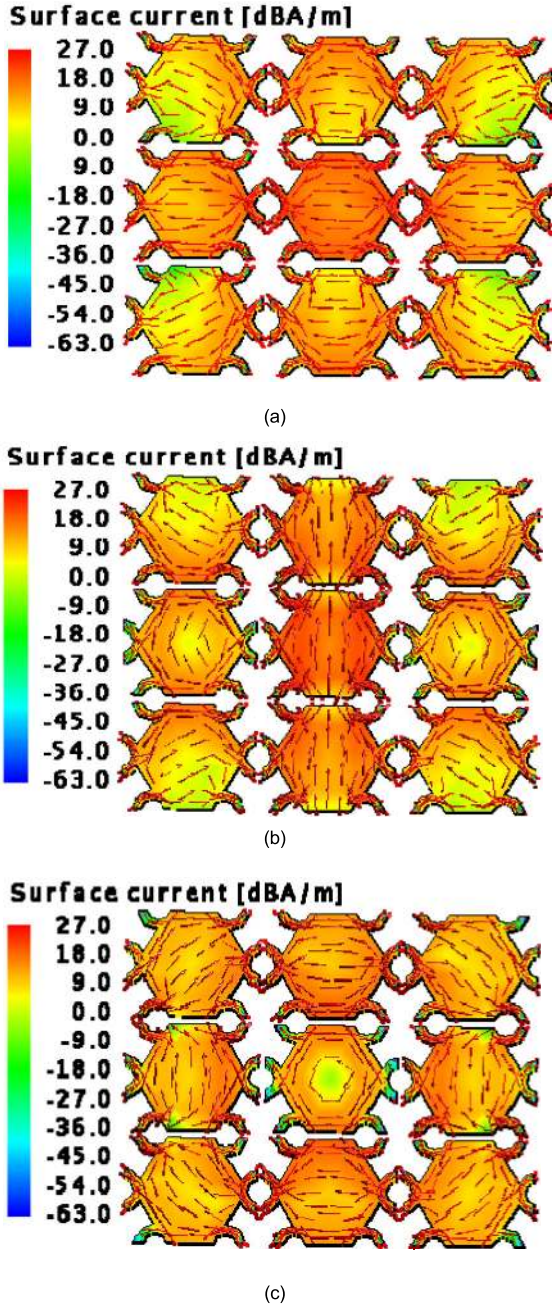

FIGURE 19. Surface current visualization of 3 × 3 array of AMC unit cells at different modes (a) mode1 (b) mode 2 (c) mode 3.

difference of material properties in practice and the effect of the SMA connector. The 2-D far-field patterns presented the watch strap antenna considering the influence of the wrist. The results corresponding to the structure of the watch strap partially or completely in contact with the wrist skin together. The CPA has appropriately connected to the width and the shape of the strap, and it shows mild ups and downs. Moreover, the feeding structure of the CPA is placed in a way that does not contradict the strap at the two sides of the antenna, which makes it a good candidate and adaptive for the IoT and other on body applications. Furthermore, the watch strap

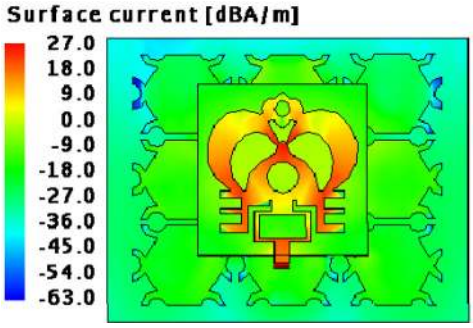

FIGURE 20. Current distribution on the CPA with 3 × 3 AMC surface.

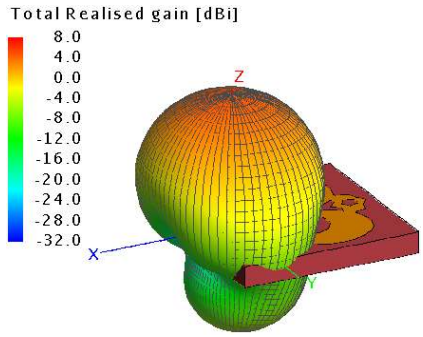

(a)

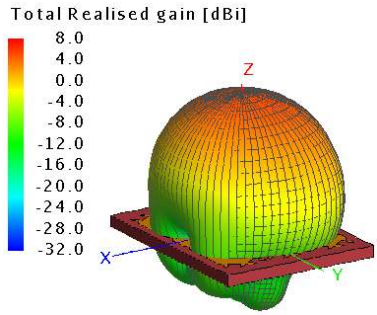

(b)

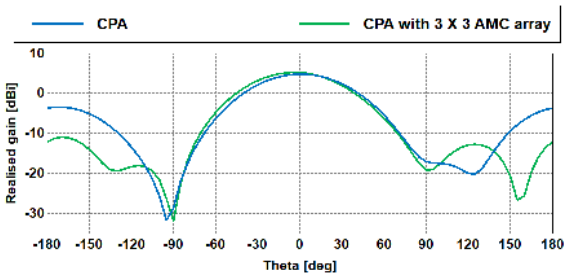

(c)

FIGURE 21. (a) 3D plot realized gain of CPA without AMC (b) 3D plot realized gain of CPA with AMC (c) 2D plot realized gain of CPA with and without AMC.

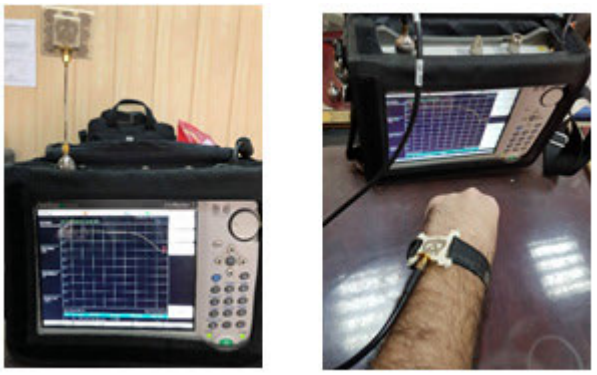

(a) (b)

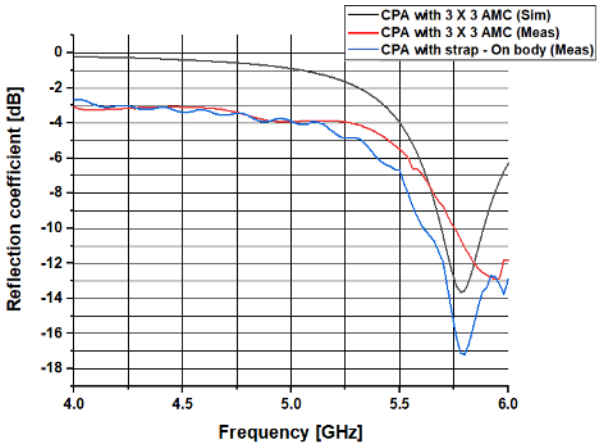

(c)

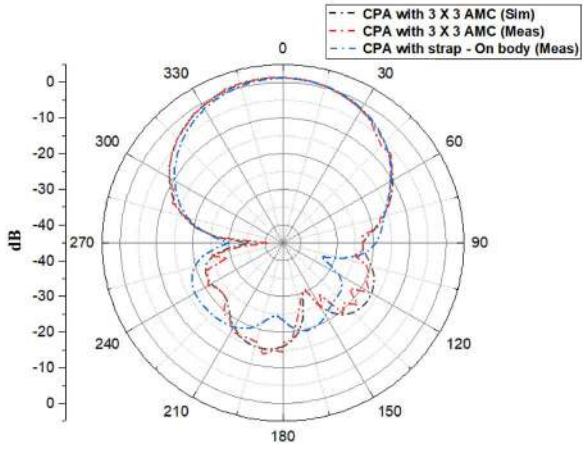

(d)

FIGURE 22. Fabricated and measurement results (a) CPA with 3 × 3 AMC surface (b) CPA with strap watch (c) reflection coefficient (d) radiation pattern.

that is connected to the CPA has not impacted the working frequency of the antenna, maintained around 5.8 GHz which falls into the ISM Band. Besides that, the impedance bandwidth of the antenna is broadened which yields to more than 380 MHz.

The simulated radiation patterns of overall antenna configurations in two principle cut planes; ($\phi = 0°$) and ($\phi = 90°$) are presented as shown in Fig. 23.

For wearable antennas, the FBR factor is critical and effectiveness in back radiation reduction. The simulated FBR

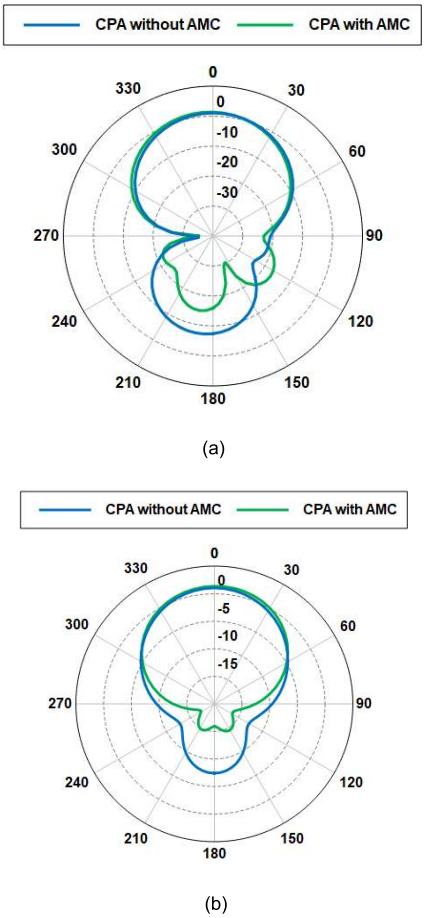

FIGURE 23. Simulated radiation patterns in the xz plane with and without the AMC plane at: $(a)\phi = 0°(b) : \phi = 90°$.

TABLE 7. FBR at different degree of phi aT 5.8 GHz.

Design structure	$\Phi = 0^{o}$	$\Phi = 90^{o}$
CPA without AMC	8.47	8.45
CPA with 3 × 3 AMC array	17.27	17.27

is observed to be larger than 12 dB in all the operational frequency bands of the antenna when printed over the AMC structure, with a maximum FBR of 17.33 dB at 5.8 GHz. Measurements indicated that the CPA with a 3 x 3 AMC plane featured an FBR of 15.73 dB. A summary of all FBR values is presented in Table 7.

The antenna presented in this paper is compared with recent state-of-art antennas, as illustrated in Table 8. The comparison is made specifically with wearable antennas operating in the 5.8 GHz band implementing AMC reflectors. Physical dimension comparison in terms of wavelength at the lowest operating frequency with antennas in the literature indicated that the proposed antenna featured a more compact size relative to [26] and [28]. Besides that, the gain obtained by the proposed antenna is also improved compared with those presented in [26]–[29], and [30] at 5.8 GHz. Moreover, the obtained FBR in this work is also improved compared

TABLE 8. Comparison of design 3 with related state-of-art literature.

Ref	Resonant frequency (GHz)	Dimensions ($\lambda g^2/mm^2$)	AMC unit cell	FBR (dB)	Gain (dBi)
[26]	2.4/5.8	1.93 × 1.93/ 147 × 147	3 × 3	11.96/ 17.46 (Sim)	3.58/6.08 (Sim)
[27]	2.45/5.8	1.17/120 (length)	8 × 8	22.4/ 12.3 (Sim)	8.6/3.7 (Sim)
[28]	3.5/5.8	1.75 × 1.75/ 86 × 86	4 × 4	7/11.3 (Sim)	9.07/7.66 (Sim)
[29]	3.5/5.8	0.58 × 0.58/ 45.3 × 45.3	2 × 2	22 (*xy* plane) 18 (*yz* plane (Sim)	6.71/7.82 (Sim)
[30]	2.45/5.8	0.38 × 0.57/ 42 × 63	2 × 3	-----	5.6/7.8 (Sim)
Proposed	5.8	1.22 × 0.95/ 55 × 43	3 × 3	17.33 (Sim) 15.73 (Meas)	8 (Sim)

λg = lower guided operating wavelength, Sim = simulated, Meas = measured.

with [27] and [28]. These improvements, in combination with the existing low profile, lightweight, and flexibility will make the proposed antenna an attractive offering to the antennas WBAN applications.

V. CONCLUSION

An efficient method of predicting the gain and directivity of three compact and planar textile wearable antennas with and without AMC for WBAN applications is presented. This method, known as the active mode subtraction method, is derived based on the characteristic mode analysis. To estimate the forward directivity, the difference in modal significance curves are computed. The total radiated field of the antenna, and consequently, the directivity is mainly contributed by the excited dominant modes. This improved the efficiency of the optimization of the antenna gain in the antenna design process. The three wearable antennas used to validate this method are made fully using textiles using felt as their substrates and ShieldIt Super as the conductive textile. Moreover, these antennas are chosen to vary in terms of design complexity, and include a simple circular patch antenna, a planar loop antenna and a crown-shaped planar antenna. Besides that, the final antenna is also integrated with diamond-shaped AMC unit cells with arched burrs, which is also optimized using the CMA method. Comparison with results generated using MoM indicated the gain and directivity of all three antennas can be predicted accurately using the proposed method. These results are then used to optimize the directivity and realized gains towards the intended direction. For instance, the simulation and measurement results obtained using this method for the final antenna indicated an improved FBR of 17.33 dB and 15.73 dB, respectively. Comparison of the proposed antenna with the state-of-the-art

wearable antennas designed with AMC planes indicated improvements in terms of gain, directivity, and size compactness, making it suitable for off-body wearable applications.

REFERENCES

[1] H. S. Girija, R. Sudhakar, K. M. A. Kadhar, T. S. Priya, S. Ramanathan, and G. Anand, "PSO based microstrip patch antenna design for ISM band," in *Proc. 6th Int. Conf. Adv. Comput. Commun. Syst. (ICACCS)*, Coimbatore, India, Mar. 2020, pp. 1209–1214, doi: 10.1109/ICACCS48705.2020.9074290.

[2] E. Li, X. J. Li, and Q. Zhao, "A design of ink-printable triband slot microstrip patch antenna for 5G applications," in *Proc. 4th Austral. Microw. Symp. (AMS)*, Sydney, NSW, Australia, Feb. 2020, pp. 1–2, doi: 10.1109/AMS48904.2020.9059378.

[3] M. Nesasudha, "A compact wearable 2.45 GHz antenna for WBAN applications," in *Proc. 5th Int. Conf. Devices, Circuits Syst. (ICDCS)*, Coimbatore, India, Mar. 2020, pp. 184–187, doi: 10.1109/ICDCS48716.2020.243577.

[4] A. Sabban, "Small new wearable metamaterials antennas for IOT, medical and 5G applications," in *Proc. 14th Eur. Conf. Antennas Propag. (EuCAP)*, Krakow, Poland, Mar. 2020, pp. 1–5.

[5] S.-H. Li and J.-S. Li, "Smart patch wearable antenna on jeans textile for body wireless communication," in *Proc. 12th Int. Symp. Antennas, Propag. EM Theory (ISAPE)*, Hangzhou, China, Dec. 2018, pp. 1–4, doi: 10.1109/ISAPE.2018.8634084.

[6] N. Singh, V. Singh, R. Saini, J. P. Saini, and A. Bhoi, "Microstrip textile antenna with Jeans substrate with applications in S-band," in *Proc. Adv. Commun., Devices Netw.*, Singapore, May 2018, pp. 369–376, doi: 10.1007/978-981-10-7901-6_40.

[7] B. Zhang, P. Yao, and J. Duan, "Gain-enhanced antenna backed with the fractal artificial magnetic conductor," *IET Microw., Antennas Propag.*, vol. 12, no. 9, pp. 1457–1460, Jul. 2018, doi: 10.1049/iet-map.2017.1130.

[8] A. Kumar, P. Kumar, and D. R. Sona, "Design of aperiodic artificial magnetic conductor in patch antenna for microwave frequencies," in *Proc. Int. Conf. Vis. Towards Emerg. Trends Commun. Netw. (ViTECoN)*, Vellore, India, Mar. 2019, pp. 1–6, doi: 10.1109/ViTECoN.2019.8899675.

[9] A. Ghosh and S. Das, "Design of broadband patch antenna with enhanced gain by using defected ground artificial magnetic conductor," in *Proc. Int. Conf. Commun. Signal Process. (ICCSP)*, Vellore, India, Apr. 2017, pp. 1364–1368, doi: 10.1109/ICCSP.2017.8286607.

[10] R. Garbacz and R. Turpin, "A generalized expansion for radiated and scattered fields," *IEEE Trans. Antennas Propag.*, vol. AP-19, no. 3, pp. 348–358, May 1971, doi: 10.1109/TAP.1971.1139935.

[11] R. Harrington and J. Mautz, "Theory of characteristic modes for conducting bodies," *IEEE Trans. Antennas Propag.*, vol. AP-19, no. 5, pp. 622–628, Sep. 1971, doi: 10.1109/TAP.1971.1139999.

[12] R. Harrington and J. Mautz, "Computation of characteristic modes for conducting bodies," *IEEE Trans. Antennas Propag.*, vol. AP-19, no. 5, pp. 629–639, Sep. 1971, doi: 10.1109/TAP.1971.1139990.

[13] J. E. Bauer and P. K. Gentner, "Characteristic mode analysis of a circular polarised rectangular patch antenna," in *Proc. 13th Eur. Conf. Antennas Propag. (EuCAP)*, Krakow, Poland, Apr. 2019, pp. 1–3.

[14] W. Li, Y. Liu, J. Li, L. Ye, and Q. H. Liu, "Modal proportion analysis in antenna characteristic mode theory," *Int. J. Antennas Propag.*, vol. 2019, pp. 1–10, Feb. 2019, doi: 10.1155/2019/7069230.

[15] V. Mahalwar and Y. K. Choukiker, "Study of radiation patterns of circular patch antenna at different modes," in *Proc. IEEE Int. Conf. Electr., Instrum. Commun. Eng. (ICEICE)*, Karur, India, Apr. 2017, pp. 1–3, doi: 10.1109/ICEICE.2017.8192445.

[16] M. L. Pablo-Gonzalez, M. Sanchez-Fernandez, and E. Rajo-Iglesias, "Combination of the three types of diversity to design high-capacity compact MIMO terminals," *IEEE Antennas Wireless Propag. Lett.*, vol. 13, pp. 1309–1312, Jul. 2014, doi: 10.1109/LAWP.2014.2336174.

[17] J. Jayasinghe, J. Anguera, and D. Uduwawala, "Genetic algorithm optimization of a high-directivity microstrip patch antenna having a rectangular profile," *Radioengineering*, vol. 22, no. 3, pp. 700–707, Sep. 2013.

[18] P. Rocca, L. Manica, and A. Massa, "Directivity optimization in planar sub-arrayed monopulse antenna," *Prog. Electromagn. Res. Lett.*, vol. 4, pp. 1–7, May 2008, doi: 10.2528/PIERL08042601.

[19] C. Saetiaw, C. Taonok, and S. Summart, "Design of modified-circular patch antenna with AMC reflector for WLAN applications," in *Proc. 15th Int. Conf. Electr. Eng./Electron., Comput., Telecommun. Inf. Technol. (ECTI-CON)*, Chiang Rai, Thailand, Jul. 2018, pp. 213–216, doi: 10.1109/ECTICon.2018.8619886.

[20] D. Sievenpiper, L. Zhang, R. F. J. Broas, N. G. Alexopolous, and E. Yablonovitch, "High-impedance electromagnetic surfaces with a forbidden frequency band," *IEEE Trans. Microw. Theory Techn.*, vol. 47, no. 11, pp. 2059–2074, Nov. 1999, doi: 10.1109/22.798001.

[21] Q. Liu, H. Liu, W. He, and S. He, "A low-profile dual-band dual-polarized antenna with an AMC reflector for 5G communications," *IEEE Access*, vol. 8, pp. 24072–24080, 2020, doi: 10.1109/ACCESS.2020.2970473.

[22] A. N. D. Silva, R. G. G. D. Carvalho, A. G. D'Assunção, Jr., and A. G. D'Assunção, "A new technique using axially slotted microstrip line for antenna impedance matching designs," *J. Microw., Optoelectron. Electromagn. Appl.*, vol. 18, no. 2, pp. 208–218, Jun. 2019, doi: 10.1590/2179-10742019v18i21556.

[23] A. H. Rambe, E. Marlianto, M. N. Nasruddin, and F. Arnia, "Optimizing rectangular patch antenna with microstrip line feed using single stub," *Int. J. Eng. Res. Technol.*, vol. 2, no. 12, pp. 1599–1602, Dec. 2013.

[24] H. Azeez, H.-C. Yang, and W.-S. Chen, "Wearable triband E-shaped dipole antenna with low SAR for IoT applications," *Electronics*, vol. 8, no. 6, p. 665, Jun. 2019, doi: 10.3390/electronics8060665.

[25] R. K. Verma and D. K. Srivastava, "Design and analysis of triple-band rectangular microstrip antenna loaded with notches and slots for wireless applications," *Wireless Pers. Commun.*, vol. 114, no. 2, pp. 1847–1864, May 2020, doi: 10.1007/s11277-020-07452-6.

[26] M. N. Ramli, P. J. Soh, M. F. Jamlos, H. Lago, N. M. Aziz, and A. A. Al-Hadi, "Dual-band wearable fluidic antenna with metasurface embedded in a PDMS substrate," *Appl. Phys. A, Solids Surf.*, vol. 123, no. 2, pp. 1–7, Feb. 2017, doi: 10.1007/s00339-017-0754-3.

[27] A. Dey, S. Bhattacharjee, S. R. B. Chaudhuri, and M. Mitra, "A dual band flexible antenna on AMC ground for wearable applications," in *Proc. IEEE Asia–Pacific Microw. Conf. (APMC)*, Singapore, Dec. 2019, pp. 607–609, doi: 10.1109/APMC46564.2019.9038804.

[28] M. El Atrash, M. A. Abdalla, and H. M. Elhennawy, "A wearable dual-band low profile high gain low SAR antenna AMC-backed for WBAN applications," *IEEE Trans. Antennas Propag.*, vol. 67, no. 10, pp. 6378–6388, Oct. 2019, doi: 10.1109/TAP.2019.2923058.

[29] M. El Atrash, M. A. Abdalla, and H. M. Elhennawy, "A fully-textile wideband AMC-backed antenna for wristband WiMAX and medical applications," *Int. J. Microw. Wireless Technol.*, pp. 1–10, Oct. 2020, doi: 10.1017/S1759078720001397.

[30] A. Mersani, O. Lotfi, and J.-M. Ribero, "Design of a textile antenna with artificial magnetic conductor for wearable applications," *Microw. Opt. Technol. Lett.*, vol. 60, no. 6, pp. 1343–1349, Jun. 2018, doi: 10.1002/mop.31158.

BASHAR BAHAA QAS ELIAS (Member, IEEE) received the B.S. degree in electrical engineering from AL-Mustansiriya University, Baghdad, Iraq, in 2011, and the M.S. degree in electrical and electronic engineering from Eastern Mediterranean University, Famagusta, North Cyprus, in 2014. He is currently pursuing the Ph.D. degree in communication engineering with the University of Perlis, Malaysia. His current research interests include microwave and millimeter-wave antennas, electromagnetic bandgap and defected ground structures, microwave metamaterial, wearable antenna, and reconfigurable microstrip circuits.

PING JACK SOH (Senior Member, IEEE) was born in Sabah, Malaysia. He received the B.Eng. and M.Eng. degrees in electrical engineering (telecommunication) from Universiti Teknologi Malaysia (UTM), in 2002 and 2006, respectively, and the Ph.D. degree in electrical engineering from KU Leuven, Belgium, in 2013.

He was a Test Engineer with Venture Corporation, from 2002 to 2004, and a Research and Development Engineer with Motorola Solutions Malaysia, in 2005. Since 2006, he has been joined SCCE-UniMAP as a Lecturer, and served as the Deputy Director of the Centre for Industrial Collaboration (CIC) from 2007 to 2009. He went on leave from UniMAP in 2009 to pursue his Ph.D. at KU Leuven. He was first a Research Assistant from 2009 to 2013, then a Postdoctoral Research Fellow from 2013 to 2014. He is currently an Associate Professor with the Faculty of Electronic Engineering Technology, UniMAP, and a Research Affiliate with KU Leuven. He is also a Research Affiliate with the ESAT-TELEMIC Research Division. Upon his return to UniMAP in 2014 as a Senior Lecturer, he concurrently served as the Deputy Dean of the university's Research Management and Innovation Center (RMIC) from 2014 to 2017. He was also the Head of the Advanced Communication Engineering (ACE) Research Centre, UniMAP, in 2020. His research interests include wearable antennas, pico-satellite antennas, flexible metasurfaces, on-body communication, electromagnetic safety, and absorption, and wireless and radar techniques for healthcare applications. He is also an Associate Editor of the *International Journal of Numerical Modeling: Electronic Networks, Devices, and Fields* (Wiley).

Dr. Soh was a recipient of the IEEE Antennas and Propagation Society (AP-S) Doctoral Research Award, in 2012, the IEEE Microwave Theory and Techniques Society (MTT-S) Graduate Fellowship for Medical Applications, in 2013, and the International Union of Radio Science (URSI) Young Scientist Award, in 2015. He was also the Second Place Winner of the IEEE Presidents' Change the World Competition, in 2013. Two of his (co)authored journals were awarded the IEEE AP/MTT/EMC Malaysia Joint Chapter's Best Paper Award, in 2018 and 2019, and another two journals were also awarded the CST University Publication Award, in 2012 and 2011. He is a Chartered Engineer registered with the U.K., Engineering Council, a Professional Technologist registered with the Malaysia Board of Technologist (MBOT), a member of the Institution of Engineering and Technology (IET), a member of the International Union of Radio Science (URSI), and a Graduate Member of the Board of Engineers Malaysia (BEM). He also serves in the IEEE MTT-S Education Committee and the IEEE MTT-S Meetings and Symposia (M&S) Committee.

AZREMI ABDULLAH AL-HADI (Senior Member, IEEE) was born in MI, USA. He received the M.Sc. degree in communication engineering from Birmingham University, U.K., in 2004, and the D.Sc. degree in technology from Aalto University, Finland, in 2013.

He is currently working as an Associate Professor and holds a position as the Dean of the Faculty of Electronic Engineering Technology, Universiti Malaysia Perlis (UniMAP), where he has been with the School of Computer and Communication Engineering, since 2002. His current research interests include design and performance evaluation of multielement antennas, mobile terminal antennas and their user interactions, and wireless propagation.

Dr. Al-Hadi is active in volunteering work with the IEEE Malaysia Section, acting as the Vice Chair of the IEEE Antenna Propagation/ Microwave Theory Techniques/Electromagnetic Compatibility (AP/MTT/EMC) Malaysia Chapter, and the Counselor of the IEEE UniMAP Student Branch. He is a Chartered Engineer of the Institution of Engineering and Technology (IET), U.K., a Professional Technologist of the Malaysia Board of Technologist (MBOT), a member of the Board of Engineers Malaysia (BEM), Malaysia. He was a recipient of the Best Student Paper Award presented at the Fifth Loughborough Antennas and Propagation Conference (LAPC 2009) and the CST University Publication Award, in 2011.

PRAYOOT AKKARAEKTHALIN (Member, IEEE) received the B.Eng. and M.Eng. degrees in electrical engineering from the King Mongkut's University of Technology North Bangkok (KMUTNB), Bangkok, Thailand, in 1986 and 1990, respectively, and the Ph.D. degree from the University of Delaware, Newark, DE, USA, in 1998.

From 1986 to 1988, he was a Research and Development Engineer with Microtek Company Ltd., Thailand. In 1988, he joined the Department of Electrical and Computer Engineering, Faculty of Engineering, KMUTNB, where he is currently the Head of the Wireless Communication Research Group (WCRG), Department of Electrical and Computer Engineering. He has authored or coauthored more than 60 international journals, more than 300 conference papers, and five books/book chapters. His current research interests include RF/microwave circuits, wideband and multiband antennas, telecommunications, and electromagnetic-based sensor networks and systems. He is a member of IEICE Japan, ECTI, and EEAAT Associations Thailand. He was the Editor-in-Chief of the *ECTI Transactions*, from 2011 to 2013, the Chairman of the IEEE MTT/AP/ED Thailand Joint Chapter, from 2007 to 2010, the Vice President of the *ECTI Association*, Thailand, from 2012 to 2013, and the President of the ECTI Association, Thailand, from 2014 to 2015. He was the Leader of Thailand Senior Research Scholar Projects of Electromagnetic Applications for Sustainable Development in Thailand Industry from 2014 to 2017 and Innovative Sensor Technology using Electromagnetics for Thailand Development from 2017 to 2020 granted by the Thailand Research Fund (TRF), Thailand.